CFD STUDY OF A MICRO AIR VEHICLE (MAV)

L.Y. Shern[1], F. A. Z. Mohd Sa'at[1,2,3] and M. A. Abdul Wahap[2,4]

[1]Faculty of Mechanical Engineering,Universiti Teknikal Malaysia Melaka, Hang Tuah Jaya, 76100 DurianTunggal, Melaka, Malaysia.

[2]Centre for Advanced Research on Energy, Universiti Teknikal Malaysia Melaka, Hang Tuah Jaya, 76100 Durian Tunggal, Melaka, Malaysia.

[3]Centre of Excellence Geopolymer and Green Technology, Universiti Malaysia Perlis, 01000 Kangar, Perlis, Malaysia.

[4]Faculty of Mechanical and Manufacturing Engineering Technology, Universiti Teknikal Malaysia Melaka, Hang Tuah Jaya, 76100 Durian Tunggal, Melaka, Malaysia.

Corresponding Author's Email: fatimah@utem.edu.my

Article History: Received 3 August 2021; Revised 1 October 2022; Accepted 11 January 2022

ABSTRACT: Micro Air Vehicle (MAV) is a new type of aircraft technology that is maturing day by day and has recently reached unprecedented levels of growth. MAV is small in size and provides enormous potential in many applications, both for military and civilian use. There are three types of MAV, namely rotary wing, flapping wing and fixed wing. Due to their small size, MAV faces difficulty in flying properly due to atmospheric perturbations. This study aims to model a suitable fixed-wing MAV using Computational Fluid Dynamics (CFD) to investigate the lift coefficient, drag coefficient and lift-to-drag ratio when MAV is used in perturbed flow conditions. When there is wind disturbance, the simulation results show that the lift and drag coefficient for several angles of attack changes. However, the lift-to-drag ratio seems unaffected. Results showed that MAV is best operated at an 8° angle of attack as it provides the maximum lift-to-drag ratio for situations without and with the presence of wind disturbances. The fluid dynamics behavior of flow around MAV is also discussed accordingly. Even though MAV is small in size, it is found that vortex or vorticity flow also exists in MAV, especially at a high degree angle of attack.

KEYWORDS: *Micro Air Vehicle (MAV); Computational Fluid Dynamics (CFD); fixed-wing; wind disturbances*

1.0 INTRODUCTION

Micro air vehicles (MAV) are a relatively new technology and are currently undergoing rapid growth of research developments [1]. Research related to MAV had been carried out in the countries such as the United States, Japan and China as early as the 19th century. According to Michelson, an American nonprofit institution, RAND Corporation, which helps in improving policy and making decisions through research and analysis, founded the MAV feasibility study in 1994 and concluded that MAV had great potential for military applications [2]. MAV were first defined by the US Defense Advanced Research Projects Agency (DARPA) in 1997 as unmanned aircraft that are less than 15 centimeters or 6 inches in any dimension [3]. Nowadays, the target dimension and development of insect-sized aircraft are reportedly expected in the near future. However, according to Hassanalian and Abdelkefi, they state that the dimension for MAV can also be considered to be within 15 cm to 1 m [4]. Besides, Aboelezz et al. also mentioned that MAVs should have weight in the range between 50 g to 2 kg and a flight endurance of 20 minutes should be expected [5]. Also, the materials used to build MAV should be as light as possible to reduce the burden of its weight [6].

MAV are also categorised as a small kind of unmanned air vehicles (UAV) which are used for surveillance, reconnaissance, armed attacking, search and rescue operations, as well as for transportation and scientific research [7]. MAV can be remotely or autonomously controlled without a human operator on board [8]. Basically, MAV are smaller in size and weight compared to UAV. Because of their smaller size, the probability of MAV being intercepted by radar is low, and therefore, they are manufactured for several missions. They can reach a maximum travel speed of 20 m/s and is suitable for day and night usage [9]. Thus, they are very suitable for military surveillance applications and image recording. Besides, MAV also produces lower noise when functioning and have lower production cost compared to the UAV. In addition, MAV can be operated at Reynolds numbers of up to 200000, depending on the size and types of MAV [10].

MAV has the potential to be used in urban applications to monitor traffic flow and mapping areas. MAV can also be used to observe the weather condition and provide real-time tracking of the current

location with the installation of gradient sensors and flight control feedback, which provides weather updates from time to time to the community [11]. Nowadays, MAVs are developed with great improvements in designs with advanced features of computer-aided technology, power supply with better battery technology, and visual communications with better transmitters and receivers [12]. There are various types of MAV, such as rotary wings, flapping wings and fixed wings. They are all now in existence, and each of them contains specific capabilities and limitations.

Rotary wing MAVs, as shown in Figure 1, are basically functionally similar to the concept of helicopters; the lift and thrust are generated by the spinning of rotor blades. The surface area of rotors would determine the magnitude of the supplied aerodynamic forces. When the rotors are spinning in opposite directions in a balanced manner, the rotary wing MAV can be easily stabilized, and the rotation of downwash air will be minimized [13]. Thus, the movement can be easily controlled and piloted by the users. In addition, the generation of both lift and thrust could also be increased by using multiple sets of rotors, such as quadrotors.

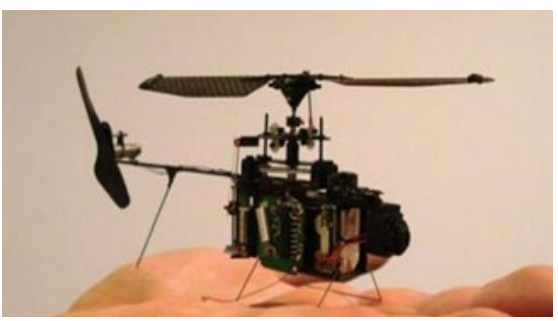

Figure 1: Sample of rotary wing MAV [13]

The flapping wing MAVs, which are also known as the biomimetic MAVs, are bioinspired with the ideas from the flapping wings of insects and birds. A sample of this MAV is shown in Figure 2. Flapping wing MAV is relatively smaller in size compared to the others, and it is more suitable for indoor applications due to its ability to fly through a narrow gap. It is more complex and complicated to be built as it consists of lightweight structures and small-scale electronic devices. Lift and thrust are achieved by flapping the wings, and the

corresponding flapping frequency depends on the surface area of the wings [13].

Figure 2: Sample of flapping wing MAV [13]

Figure 3 shows another type of MAV, known as a fixed-wing MAV, which may not be very suitable for indoor usage. It is more suitable for outdoor surveillance missions since they have higher payload and endurance capabilities compared to rotary and flapping wing MAVs of equal size [13]. A propeller-driven electrical motor is normally used in fixed-wing MAV to produce thrust. Lift is generated by air flowing over the non-moving wings of airfoil cross sections. Fixed-wing MAVs have difficulties achieving good performances at low-speed flights as their wings are associated with stringent dimension constraints requiring high cruise speeds.

Figure 3: Sample of fixed-wing MAV [13]

Normally, all of the MAVs are equipped with Inertial Measurement Unit (IMU) to estimate the angular velocities and accelerations of the vehicles in vertical, longitudinal and lateral axis [14]. In order to improve the flight performance of MAV, Bowles et al. and Patel et al.

stated that pressure sensors could be implemented to predict the leading edge flow separation and also trigger plasma flow actuators for flow and attitude control of MAV [15, 16].

The small size and low operating speed of MAV lead to unique aerodynamic conditions [17]. According to Kunz, the most common problem that is faced by the MAV, is its difficulty in flying stably at low Reynolds numbers due to its small size [18]. Previous research indicated that there would be an increase in maximum lift coefficient with a decrease in Reynolds number. However, as the Reynolds number decreases, the lift-to-drag, L/D ratio also decreases. Hence more power is required to operate the flight. Therefore, flight at these Reynolds numbers is much less efficient than at higher Reynolds numbers. It is important to operate the airfoil at its maximum lift-to-drag ratio for its optimum performance [19]. Besides the limitation of the supplied power, MAV also faces technological and manufacturing challenges due to its small feature.

Flow at low Reynolds numbers is dominated by viscosity, and as the Reynolds number is reduced, the effects of increasing boundary layer thickness become more significant [20]. This leads to the effect of higher drag conditions. Thus, low Reynolds numbers affect the aerodynamic efficiency and the propulsion efficiency dramatically. These problems cause difficulty in flying the MAVs properly as they have to face sensitivity issues due to atmospheric perturbations [21]. Therefore, the lift coefficient, drag coefficient and the fluid dynamics around the MAV are important aspects to be investigated so that the MAV can function under optimized conditions.

2.0 METHODOLOGY

In this study, CATIA V5 software will be used to draw the MAV model, while ANSYS Version 16.1 CFD Fluent software will be used to carry out all relevant simulations. Previous results from the other researchers will be used as a reference to validate the simulation models. Validation is important as it would affect the accuracy of results for further study and investigation of fluid dynamics behavior on MAV under different cases, situations or conditions. Based on the number of

simulations required for the results, a sufficient and optimum volume of a computational domain that satisfied the trailing vortex flow and turbulence establishment is considered. The streamwise length of MAV, L (250 mm), is used as a measurement for the computational domain volume. The dimensions of the computational domain are identified as 1L (250 mm) before the leading edge and 3L (750 mm) after the trailing edge, whereas from the top, bottom and sides of the wing are 1.5L (375 mm). Figure 4 shows the MAV allocated inside the computational domain. The bottom picture of Figure 4 shows the 3D view of the domain with inlet and outlet boundaries.

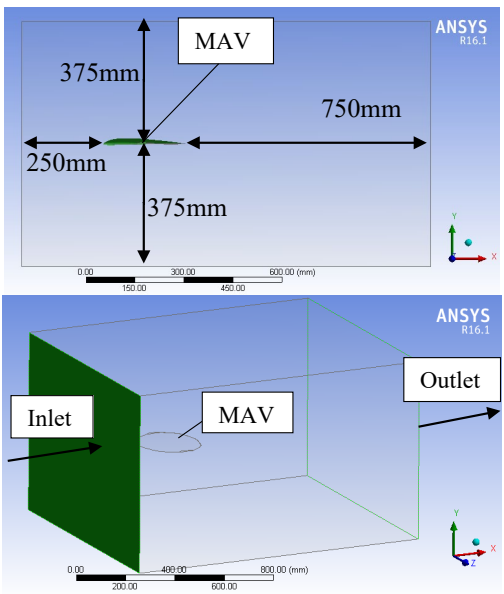

Figure 4: The side view of the computational domain with dimensions (top) and the three-dimension view of the domain (bottom)

The dimensions of the model and the types of the airfoil are obtained from NAL's Black Kite MAV by Sankaranarayanan et al. [22] as cited in Ramprasadh and Devanandh [23]. The profile of the SELIG 4083 airfoil is chosen for the wing that is investigated in the 3D model. Based on the UIUC airfoil coordinates database, SELIG 4083 airfoil has a maximum thickness of 8% at 22.5% chord and a maximum chamber of 3.4% at 33.5% chord. A 3D CAD model of the Low Aspect Ratio (LAR) wing for the fixed-wing MAV is modeled using CATIA V5. It is a Modified Inverse Zimmerman (MIZ) planform with an aspect ratio of 1.45, wingspan of 300 mm, Mean Aerodynamic Chord (MAC) of 209

mm and the center of the wing consists of a chord length of 250 mm. Figure 5 shows the CAD model of the wing from various views.

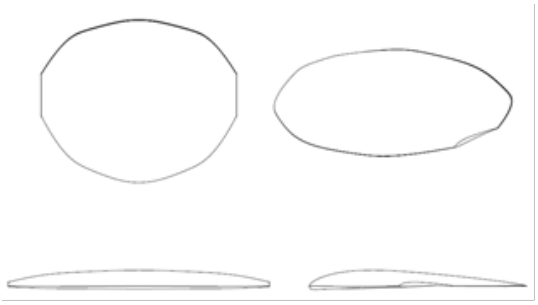

Figure 5: CAD model of wing

ANSYS CFD Fluent is used to simulate the models. The solver is set as a pressure-based type with absolute velocity formulation and a steady-state simulation. A realizable k-epsilon turbulence model with standard wall functions was employed. The properties of the fluid are treated as constant, and the values are shown in Table 1.

Table 1: Fluid properties

Properties	Value
Density (kg/m^3)	1.225
Specific Heat (J/kg.K)	1006.43
Thermal Conductivity (W/m.K)	0.242
Viscosity (kg/m.s)	1.7894e^{-5}

In boundary conditions, the velocity specification method of flow for both inlet and outlet is defined as normal to the boundary, with gauge pressures equal to zero. Besides, the walls of MAV and domain should be defined as stationary walls with the no-slip condition [24]. Table 2 summarised the baseline conditions that were solved for the current simulation.

Table 2: Flow parameters

Thermodynamic Parameters	Velocity Parameters	Turbulence Parameters
Temperature: 293.20 K Pressure: 101325 Pa	Velocity in: 1. X-direction: 12 m/s 2. Y-direction: 0 m/s 3. Z-direction: 0 m/s	Turbulence intensity: 0.10% Length: 1.00e^{-4} m

For the solution methods, the SIMPLE algorithm was used for the pressure-velocity coupling when solving the Navier-Stokes equations.

Green-Gauss Node Based gradient and second-order pressure were selected for the spatial discretization scheme. The turbulent kinetic energy, turbulent dissipation rate, momentum and energy equations are discretized by the second-order upwind method.

A grid-independent test was carried out to ensure that the simulation result was independent of the gird size. The test was done by monitoring the resulting lift coefficients from models with several mesh elements. The test was carried out for a 24° angle of attack to observe the stability of simulated lift coefficient results. The grid test results are shown in Table 3 and Figure 6.

With reference to Table 3 and Figure 6, the lift coefficient decreases with the number of elements initially until it reaches the grid size of 732207 elements. After that, the lift coefficient result is almost constant. Hence, the model, which consists of 732207 elements, is selected for use in this current study as it provides stable results with the least computational time.

Table 3: Grid test on lift coefficient at 24° angle of attack

Number of Elements	488265	522277	606548	732207	771964	777731	781601
Lift coefficient, C_L	1.138	1.134	1.130	1.125	1.125	1.125	1.126

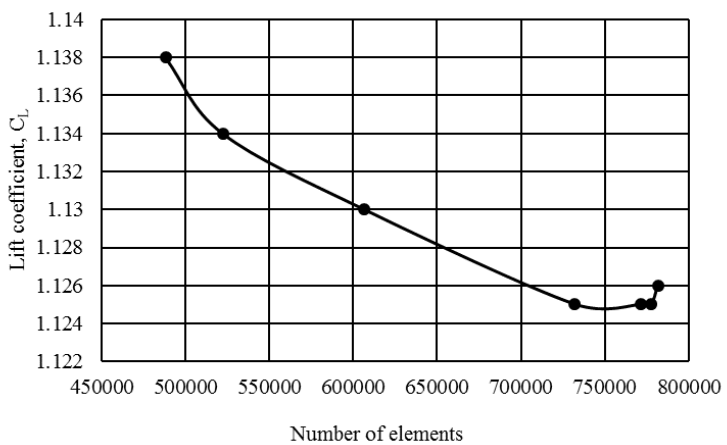

Figure 6: Lift coefficient grid test at 24° angle of attack

3.0 RESULTS AND DISCUSSIONS

3.1 Validation

For the purpose of model validation, the model was set up following the parameter used by Ramprasadh and Devanandh [23]. The data and results for lift coefficient, C_L at different angles of attack are shown in Table 4 and Figure 7, respectively.

From Table 4 and Figure 7, when the angle of attack increases, the lift coefficient also increases. This indicates that a higher amount of lift force will be generated at a higher degree angle of attack. The simulation results on the lift coefficient for this MAV model at 0°, 8°, 16°, and 24° are 0.110, 0.423, 0.760 and 1.125, respectively. The average percentage of error between results from the current model and the experimental and simulation models of Ramprasadh and Devanandh [23] is 10.30% and 11.85%, respectively. The deviation is bigger as the Reynolds number is bigger. However, the general trend of change of lift coefficient with Reynolds number is the same as predicted by Ramprasadh and Devanandh [23].

Table 4: Lift coefficient at various angles of attack

	Lift Coefficient, C_L			Percentage Error (%)	
Angle of Attack (°)	NAL Experimental Data [23]	CFD Fluent Data Results [23]	Simulation Results	Experiment	Fluent
0	0.097	0.090	0.110	13.40	22.22
8	0.425	0.420	0.423	0.47	0.71
16	0.900	0.830	0.760	15.56	8.43
24	1.275	1.340	1.125	11.76	16.04
		Average Percentage Error (%)		10.30	11.85

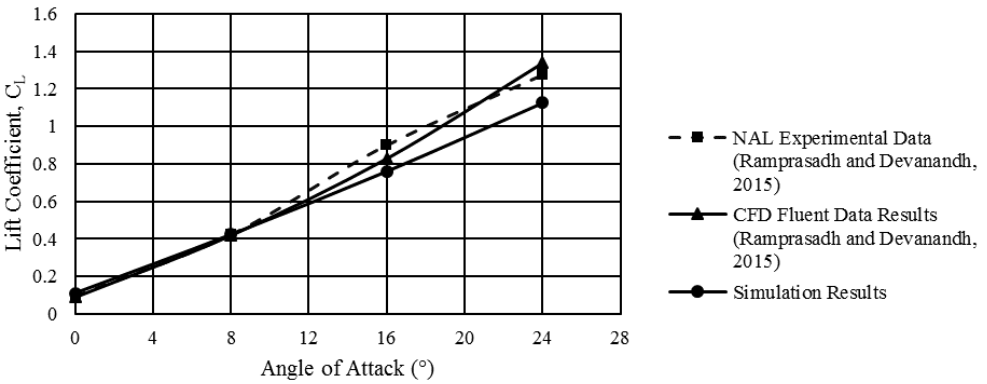

Figure 7: Lift coefficient at a different angle of attack

3.2 Fluid Dynamic Behavior

Other than the lift coefficient, the fluid dynamics behavior of flow around MAV at a different angle of attack can also be further investigated through the contours and streamline plots. For the convenience of presentation, the plots are presented in tables.

The contours of velocity and pressure for the MAV model at its middle cross section for each respective angle of attack are shown in Table 5. According to Bernoulli's principle, pressure and velocity are inversely proportional. The greater the velocity, the lower the pressure. Referring to the contours, the velocity of fluid flow is exactly as predicted, as it is greater at the low-pressure region.

As expected, the velocity of flow across the airfoil at 0° angle of the attack shows that the flow is not severely affected by the presence of the airfoil, and the velocity of flow around the airfoil is slightly lower compared to the surrounding due to the viscous effect near the surface. As the angle of attack increases, the velocity of air increases especially within the region near the leading edge. These velocity changes are the main factors that caused the pressure difference around the model. At a 24° angle of attack, the leading edge experiences a maximum velocity field with a value of around 22 m/s. Hence, the velocity of airflow within that particular region is relatively big compared to other cases of angles of attack. The ratio of lift-to-drag, L/D, for the case of 8° angle of attack, was recorded to be the best for this design of MAV with a value of 6.934. The velocity that is flowing through the upper path from

the leading edge is around 16.50 m/s, and the pressure at the leading edge is about 82.424 Pa.

The pressure contours in Table 5 show that there is a maximum pressure distribution at the leading edge of MAV model at 0° angle of attack. When the angle of attack increases, the pressure distribution at the lower path of MAV also increases. Thus, it causes a greater pressure difference between the lower path and the upper path of MAV. The differential pressure distributed around the airfoil causes lift force to be generated. Hence, the lift force generated and lift coefficient is greater at a higher degree angle of attack as the pressure at both paths is gradually changing. Besides lift, the drag force and drag coefficient also increase with the increase of the angle of attack, as there is an increment in the frontal area for the airfoil, which restricts the airflow.

The path of air that is flowing across the MAV model could also be traced through the streamlines. The results of streamlines at different angles of attack are shown in Table 6. Based on the results, the streamline from 0° angle of attack is considered as an attached flow, and the velocity is relatively constant throughout the domain. As the angle of attack increases, there is a separation of flow, and the separation of flow is slowly becoming more obvious towards the 24° angle of attack. However, the wake region is still not significant. Besides, the streamlines, after passing through the model, do not behave in a parallel flow manner. The velocity of the streamline is relatively similar to the velocity contour as discussed earlier. The maximum velocity at the leading edge is about 22 m/s at a 24° angle of attack.

In order to see the flow behaviour on the third dimension, a plane was created around the middle section of MAV in the YZ plane, as shown in Figure 8, to observe the existence of vortex or vorticity of flow at that dimension. The behavior of the flow of air can be represented by the flow vector. Again, the plots are presented in the form of a table for ease of data presentation and analysis. Based on the results shown in Table 7, the flow vector becomes more significant and forms a more obvious circular vector as the angle of attack increases. This indicates that vortex or vorticity of flow exists in the third dimension of the flow around MAV, especially at a high degree angle of attack. The flow

vector shows that the maximum magnitude is around 16.50 m/s at a 24° angle of attack for the selected area of analysis. Hence, a higher angle of attack will lead to a greater vortex or vorticity problem, which might influence the performance of MAV. Therefore, the angle of attack is an important factor that should be taken into consideration for design purposes.

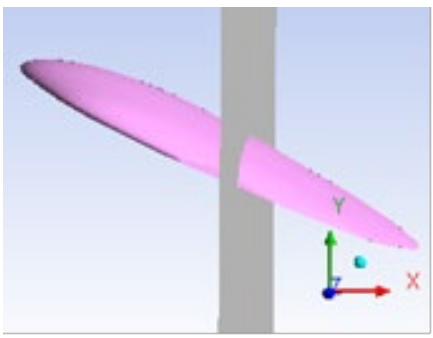

Figure 8: Side view of MAV at 24° angle of attack

3.3 The Impact of Wind Disturbances

Considering that the MAV is operating under an actual condition where the cruise takes place in uncertain flow conditions and with the presence of wind disturbances, additional investigation is carried out to determine whether the impact of wind would affect the CL, CD or the overall performance of this MAV. Typically, there are 3 cases that were investigated. First, wind disturbance of 2 m/s in both X and Z directions, respectively, where X direction is the direction that is parallel to the flow, whereas Z direction is from the side. Secondly, the wind velocity in the X direction is amplified to 5.5 m/s, and then lastly, the condition with a wind of 3 m/s coming from the Z direction was also solved. These conditions were identified based on findings from literature surveys. The conditions were stated as maximum potential disturbances which will cause the MAV to be dynamically unstable [5]. Table 8 and Figure 9 show the resulting lift coefficient of MAV under the three different situations with 4 cases of the angle of attack.

Table 5: Velocity and pressure contour at a different angle of attack

Angle of Attack (°)	Velocity Contour	Pressure Contour

Table 6: Streamlines at a different angle of attack

Angle of Attack (°)	Streamline
0	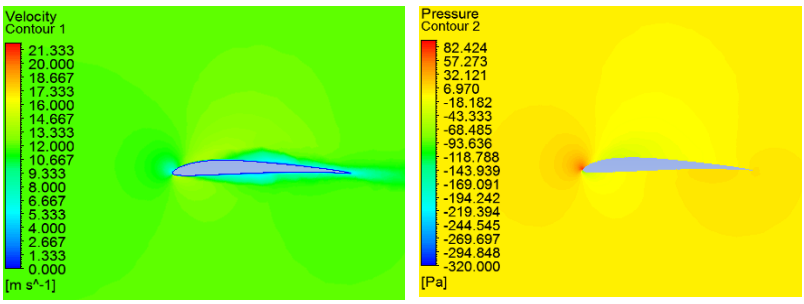
8	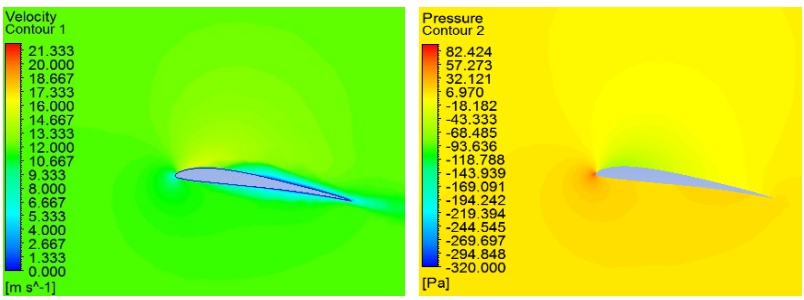
16	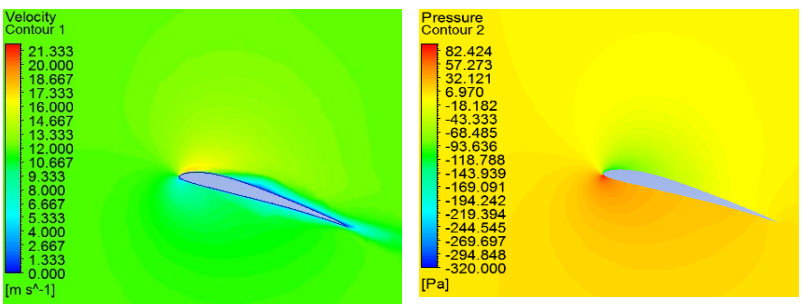
24	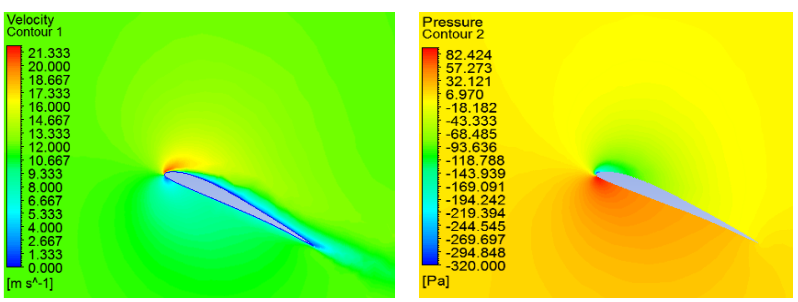

Table 7: Flow vector at a different angle of attack

Angle of Attack (°)	Flow Vector
0	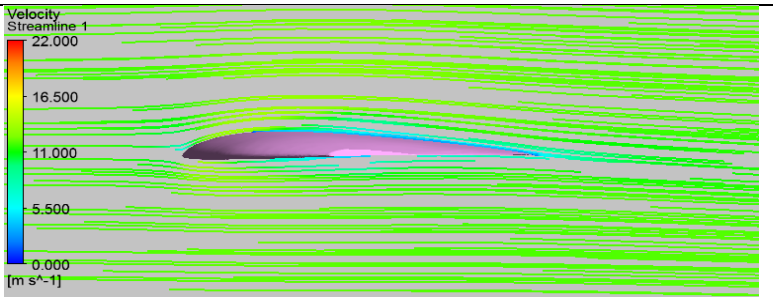
8	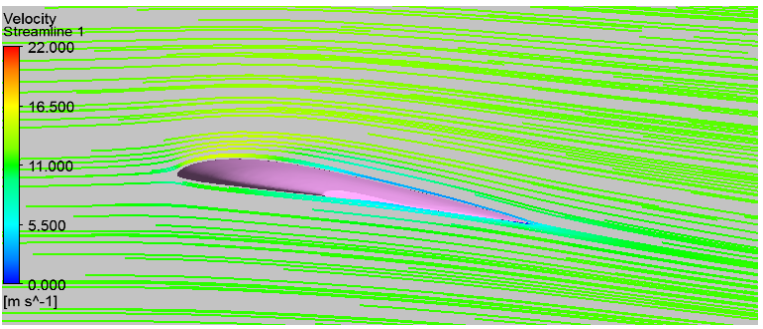
16	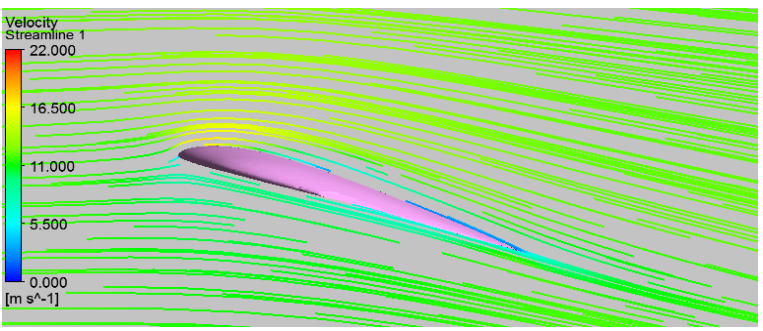
24	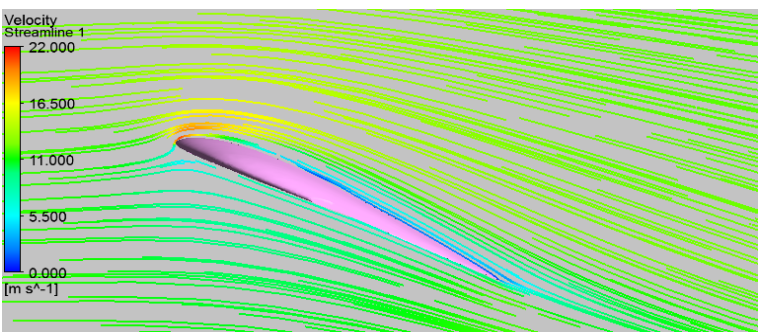

0

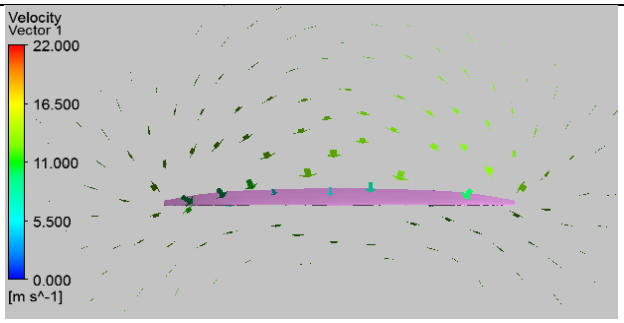

8

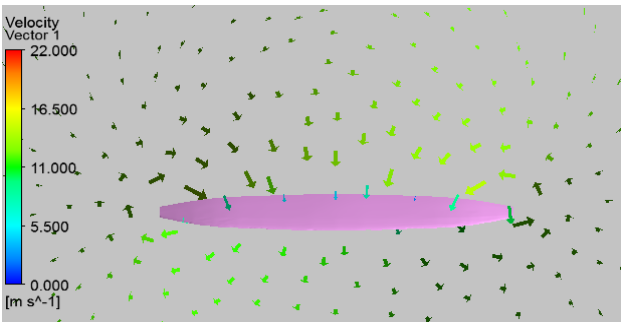

16

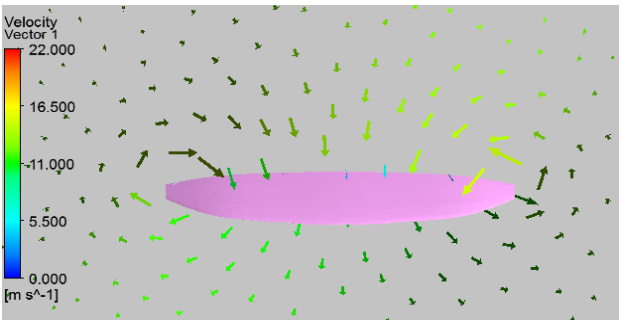

24

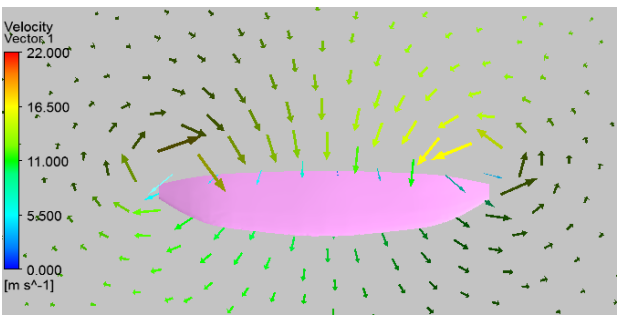

Table 8: Lift coefficient in a different situation

		Lift Coefficient, C_L		
Angle of	Without wind	Wind in (X,Z),	Wind in X,	Wind in Z,

Attack (°)	disturbance	2 m/s	5.5 m/s	3 m/s
0	0.110	0.110	0.168	0.086
8	0.423	0.420	0.424	0.204
16	0.760	0.750	1.166	0.731
24	1.125	1.108	1.129	0.539

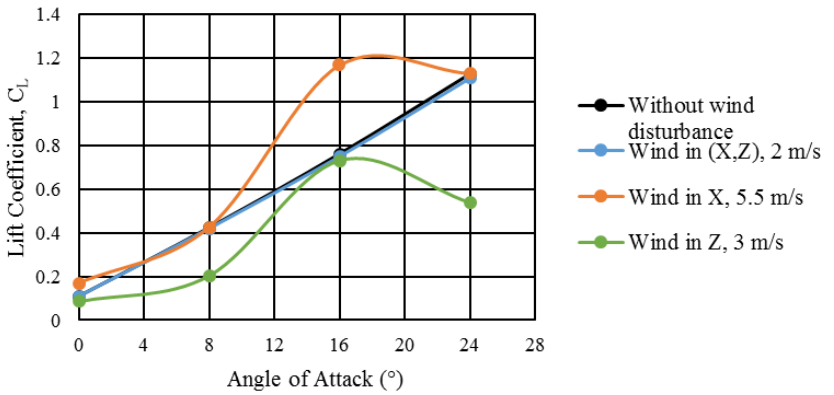

Figure 9: Lift coefficient under different situations

Results in Table 8 and Figure 9 shows that when there is wind disturbances of 2 m/s in both X and Z directions, there will be no significant effect on the CL of MAV from 0° to 24° angle of attack compared to the situation that is without any wind disturbances which was discussed earlier. However, when the wind is only coming from X direction with a higher velocity of 5.5 m/s, the CL of MAV at 16° angle of attack increases significantly to 1.129 (maximum), and it reaches a stall condition for 24° angle of attack as the CL dropped. Thus, the 16° angle of attack reflects that it is the critical angle of attack for that case. The CL will decrease once the critical angle of attack is exceeded [25]. For the wind disturbance from Z direction with a velocity of 3 m/s, the CL at 8° and 24° angles of attack are relatively lower compared to that of without wind disturbance, but the CL does not affect much at 0° and 16° angle of attack. Besides, the MAV also experienced a stalling condition at a 24° angle of attack when there was a wind of 3 m/s from the Z direction. Hence, the wind in different cases might be affecting the CL of MAV for several angles of attack.

From Table 9 and Figure 10, it seems that the wind disturbances in both X and Z directions with 2 m/s strength are still not having a big impact on the CD of MAV for all the investigated angles of attack. But when

the wind is 5.5 m/s in X direction, the CD at 16° is higher in comparison to all other cases. For the case of wind in the Z direction with 3 m/s, the CD at 8° slightly dropped, and the CD at 24° is extremely lower compared to the situation without wind disturbances. These show that the influence of wind disturbances would also affect the CD significantly depending on the situation.

Table 9: Drag coefficient in a different situation

	Drag Coefficient, C_D			
Angle of Attack (°)	Without wind disturbance	Wind in (X,Z), 2 m/s	Wind in X, 5.5 m/s	Wind in Z, 3 m/s
0	0.023	0.023	0.034	0.019
8	0.061	0.061	0.059	0.030
16	0.156	0.154	0.236	0.152
24	0.342	0.336	0.342	0.165

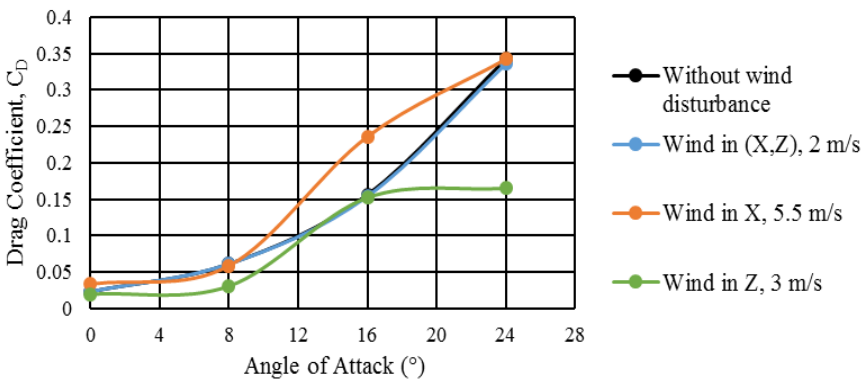

Figure 10: Drag coefficient under different situations

Table 10 and Figure 11 show the performance of MAV based on the lift-to-drag, L/D ratio. It can be seen that the L/D ratios are relatively similar for all of the investigated cases at every angle of attack. The L/D ratio is just slightly higher at 8° when 5.5 m/s wind is imposed from the X direction. Since the trend of the graph for the L/D ratio for all situations is almost the same, it can be concluded that the L/D ratio is not much affected by the presence of wind disturbances. It seems that, although the CL and CD were shown earlier to be affecting the MAV performance, the L/D ratio is not. The overall performance of MAV is still the best at an 8° angle of attack as the L/D ratio is highest between 0° to 24° angle of attack.

Table 10: Lift-to-drag ratio in a different situation

	Lift-to-Drag Ratio, L/D			
Angle of Attack (°)	Without wind disturbance	Wind in (X,Z), 2 m/s	Wind in X, 5.5 m/s	Wind in Z, 3 m/s
0	4.783	4.783	4.941	4.526
8	6.934	6.885	7.186	6.800
16	4.865	4.870	4.941	4.809
24	3.296	3.298	3.301	3.267

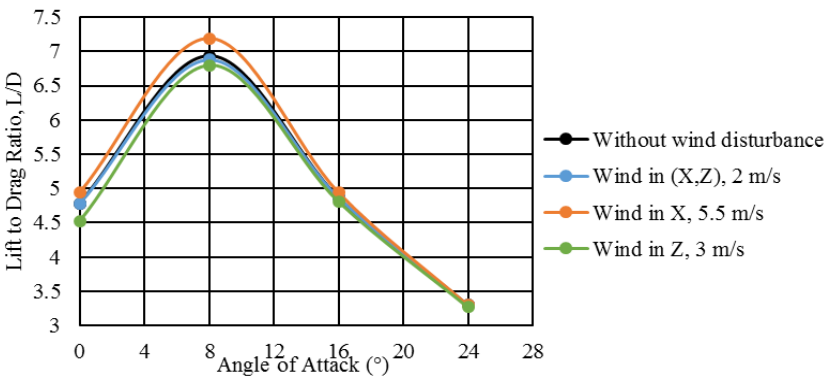

Figure 11: Lift-to-drag ratio under different situations

4.0 CONCLUSION

A computational fluid dynamics, CFD, study of the impact of flow disturbances on the performance of a fixed-wing MAV is reported. The model was first validated with a benchmarked case. The results from the validated CFD models show that the best angle of attack for this MAV model is 8° as it obtained the maximum L/D ratio compared to 0°, 16° and 24° angles of attack. Besides, as MAV is smaller in size compared to other aircraft, such as UAV, it may have sensitivity issues when operating in an actual situation. Thus, the parametric investigation is carried out to determine whether flow disturbances are giving an impact on the lift coefficient, drag coefficient and lift-to-drag ratio for this MAV model when it is operating under conditions with wind disturbances. The simulation results, it shows that the lift coefficient and drag coefficient might be influenced by the wind disturbances on some angle of attack and could cause potential stall condition. However, the lift-to-drag ratio, which determines the performance of MAV, is not affected significantly. In conclusion, this MAV model is found to be able to operate well even with disturbances (within the limitation of investigated

conditions) and had the best performance at an 8° angle of attack with the consideration of wind disturbances.

ACKNOWLEDGMENTS

The authors would like to thank Universiti Teknikal Malaysia Melaka for providing the facilities for conducting the research works.

REFERENCES

[1] D.M. Atwater, "The Commercial Global Drone Market", *Emerging Opportunities for Social and Environmental Uses of UAVs*, pp. 18, 2015.

[2] R.C. Michelson, "Very Small Flying Machines", *Yearbook of Science and Technology, McGraw-Hill, New York,* pp. 341-344, 2006.

[3] L. Petricca, P. Ohlckers, and C. Grinde, "Micro- and Nano-Air Vehicles: State of the Art", *International Journal of Aerospace Engineering*, pp. 1-17, 2011.

[4] M. Hassanalian, and A. Abdelkefi, "Classifications, Applications and Design Challenges of Drones: A Review", *Progress in Aerospace Science*, pp. 99–131, 2017.

[5] A. Aboelezz, M. Hassanalian, A. Desoki, B. Elhadidi, and G. El-Bayoumi, "Design, Experimental Investigation and Nonlinear Flight Dynamics with Atmospheric Disturbances of a Fixed Wing Micro Air Vehicle", *Aerospace Science and Technology*, vol. 97, 2020.

[6] M. Hossain, F. Hasan, A. Seraz, and S. Rajib, "Development of Design and Manufacturing of a Fixed Wing Radio Controlled Micro Air Vehicle (MAV)", *MIST Journal: GALAXY (DHAKA)*, vol.3, 2011.

[7] D. Hodgkinson, and R. Johnston, "Aviation Law and Drones", *Unmanned Aircraft and the Future of Aviation, Routledge*, 2018

[8] A. Tahir, J. Boling, M. Haghbayan, H.T. Toivonen, and J. Plosila, "Swarms of Unmanned Aerial Vehicles - A Survey", *Journal of Industrial Information Integration*, vol. 16, 2019.

[9] D.F. Kurtulus, "Unsteady Aerodynamics of a Pitching NACA 0012 Airfoil at Low Reynolds Number", *International Journal of Micro Air Vehicles*, vol. 11, 2019.

[10] T.J. Mueller, and G.E. Torres, "Aerodynamics of Low Aspect Ratio Wings at Low Reynolds Numbers with Applications", *Micro Air Vehicle Design and Optimization*, pp. 39-72, 2001.

[11] A. Panta, A. Mohamed, M. Marino, S. Watkins, and A. Fisher, "Unconventional Control Solutions for Small Fixed Wing Unmanned Aircraft", *Progress in Aerospace Sciences*, vol. 102, pp. 122-135, 2018.

[12] B. Bataille, D. Poinsot, C. Thipyopas, and J.M. Moschetta, "Fixed-Wing Micro Air Vehicles with Hovering Capabilities", *Platform Innovations and System Integration for Unmanned Air, Land and Sea Vehicles (AVT-SCI Joint Symposium)*, vol. 38, pp. 1-16, 2007.

[13] T.A. Ward, C.J. Fearday, S. Erfan, and S. Norhayati, "A Bibliometric Review of Progress in Micro Air Vehicle Research", *International Journal of Micro Air Vehicles*, pp. 1-20, 2017.

[14] G.F. Emilio, O. Alberto, B.P. Francisco, and P.C. Joan, "A Mosaicing Approach for Vessel Visual Inspection Using a Micro Aerial Vehicle", *IEEE/RSJ International Conference on Intelligent Robots and Systems (IROS)*, 2015.

[15] P. Bowles, T. Corke, and E. Matlis, "Stall Detection on a Leading-Edge Plasma Actuated Pitching Airfoil Utilizing Onboard Measurement", *47th AIAA Aerospace Sciences Meeting including The New Horizons Forum and Aerospace Exposition*, 2009.

[16] M.P. Patel, Z.H. Sowle, T.C. Corke, and C. He, "Autonomous Sensing and Control of Wing Stall Using a Smart Plasma Slat", *JAircr 2007*, pp. 27-44, 2007.

[17] X.Q. Zhang, and L. Tian, "Three-Dimensional Simulation of Micro Air Vehicles with Low Aspect Ratio Wings", *Key Engineering Materials*, vol. 339, pp. 377-381, 2007.

[18] P.J. Kunz, "Aerodynamics and Design for Ultra Low Reynolds Number Flight", *PhD thesis. Stanford: Stanford University*, 2003.

[19] M. Hassanalian, H. Khaki, and M. Khosrawi, "A New Method for Design of Fixed Wing Micro Air Vehicle", *Institution of Mechanical Engineers, Part G: Journal of Aerospace Engineering*, vol. 229, pp. 837–850, 2014.

[20] F. Hsiao, C. Lin, Y. Liu, D. Wang, C. Hsu, and C. Chiang, "Thickness Effect on Low-Aspect-Ratio Wing Aerodynamic Characteristics at a Low Reynolds Number", *Journal of Mechanics*, vol. 24, no. 3, pp. 223-228, 2008.

[21] A. Mohamed, K. Massey, S. Watkins, and R. Clothier, "The Attitude Control of Fixed-wing MAVS in Turbulent Environments", *Progress in Aerospace Sciences*, vol. 66, pp. 37-48, 2014.

[22] S. Sankaranarayanan, A. Roshan, and C. Suraj, *Technology Driven*

Programme for the Development of a Fixed wing micro Air Vehicle at NALDRIVEN, 2008.

[23] C. Ramprasadh, and V. Devanandh, "A CFD Study on Leading Edge Wing Surface Modification of a Low Aspect Ratio Flying Wing to Improve Lift Performance", *International Journal of Micro Air Vehicles*, vol. 7, no.3, pp. 361-373, 2015.

[24] T. Flint, M. Jermy, T. New, and W. Ho, "Computational Study of a Pitching Bio-inspired Corrugated Airfoil", *International Journal of Heat and Fluid Flow*, vol. 65, pp. 328-341, 2017.

[25] W. Shyy, Y. Lian. J. Tang, H. Liu, P. Trizila, B. Stanford, L. Bernal, C. Cesnik, and P. Ifju, "Computational Aerodynamics of Low Reynolds Number Plunging, Pitching and Flexible Wings for MAV Applications", *Acta Mech Sin*, vol. 24, pp. 351–373, 2008.